Aerosol Jet-Printed High-Aspect Ratio Micro-Needle Electrode Arrays Applied for Human Cerebral Organoids and 3D Neurospheroid Networks

Sabine Zips, Boxin Huang, Salammbô Hotte, Lukas Hiendlmeier, Chen Wang, Karthyayani Rajamani, Olivier Buriez, George Al Boustani, Yong Chen, Bernhard Wolfrum, et al.

Aerosol Jet-Printed High-Aspect Ratio Micro-Needle Electrode Arrays Applied for Human Cerebral Organoids and 3D Neurospheroid Networks

Sabine Zips[1]‡, Boxin Huang[2]‡, Salammbô Hotte[2]‡, Lukas Hiendlmeier[1], Chen Wang[1], Karthyayani Rajamani[2], Olivier Buriez[2], George Al Boustani[1], Yong Chen[2], Bernhard Wolfrum[1]*, Ayako Yamada[2]**

[1] Neuroelectronics - Munich Institute of Biomedical Engineering, Department of Electrical Engineering, TUM School of Computation, Information and Technology, Technical University of Munich, Boltzmannstr. 11, 85748 Garching, Germany

[2] PASTEUR, Department of Chemistry, École Normale Supérieure, PSL University, Sorbonne Université, CNRS, 75005 Paris, France

KEYWORDS: micro-needle electrode array, 3D MEA, aerosol-jet printing, inkjet printing, cerebral organoid, hiPSC-derived neural network

ABSTRACT

The human brain is a complex and poorly accessible organ. Thus, new tools are required for studying neural function in a controllable environment that preserves multicellular interaction and neuronal wiring. In particular, high-throughput methods that alleviate the need for animal experiments are essential for future studies. Recent developments of induced pluripotent stem cell technologies have enabled *in vitro* modeling of the human brain by creating three-dimensional brain tissue mimic structures. To leverage these new technologies, a systematic and versatile approach for evaluating neuronal activity at larger tissue depths within the regime of tens to hundreds of micrometers is required. Here, we present an aerosol-jet and inkjet-printing-based method to fabricate microelectrode arrays, equipped with high-aspect ratio µ-needle electrodes that penetrate 3D neural network assemblies. The arrays have been successfully applied for electrophysiological recordings on interconnected neurospheroids formed on an engineered substrate and on cerebral organoids, both derived from human induced pluripotent stem cells.

1. Introduction

The prevalence of neurodegenerative diseases in our aging society calls for novel model systems to provide insights into the brain disease mechanisms and evaluate potential strategies for treatments in a high-throughput approach. However, the mimicking of neuronal disease for experimentation and research is challenging. Animals are frequently used models for the

nervous system. However, the ethical circumstances are usually complex, the care-taking of the animals is costly, and often the translation from the animal to the human organisms fails due to their disparities. In recent years, *in vitro* systems based on human induced pluripotent stem cells (hiPSCs) have become a powerful research tool for recapitulation of neurodegenerative disease phenotypes and drug discovery, allowing us to generate functional human neural tissues.[1, 2] Besides, microstructured platforms, such as microfluidic systems and scaffolds, have been developed for *in-vitro* modelling of cell-network formation and neurodegenerative disease pathologies.[3] These culture platforms, however, produce 2D-neuronal networks grown on flat rigid surfaces sometimes with substrate-integrated sensor elements and thus, lack in properties of a real *in vivo* cellular environment, which is characterized by neuronal outgrowth in 3D dimensions, embedment into a soft extracellular matrix, and interaction with a multitude of different cell types in 3D networks.[4] These cues can drastically change the behavior of the cells such as morphology and cytoskeleton composition, neurite growth, maturation, and survival.[5-13] Thus, 3D culture methods have been developed such as encapsulation in gel, in-growth into stacked gelatin nanofiber meshes or multi-layers of glass microbeads, neurospheroids, neurospheres, and cerebral organoids.[13-20] So far, the directional outgrowth of axons in 3D cultures was mainly achieved by controlled gradients of mechanical and chemical cues, while neurospheres and cerebral organoids are known to establish self-assembled core-shell structures and are able to exhibit larger inner and outer axonal projections.[21-25]

Neural networks that recapitulate 3D features of the brain, coupled with micro-transducer arrays for electrophysiological recordings, would be an ideal tool for high-throughput investigations on neurodegenerative pathways and drug screening.[2, 4, 26, 27] Microelectrode arrays (MEAs) are frequently used tools for research on the electrophysiological behavior of cells on the network as well as at the single-cell level.[28-47] Fair, *et al.* demonstrated successful recordings of extracellular signals at the surface of a cerebral organoid by 2D MEA with planar electrodes,

which allowed long-term analyses of the evolution of the electrophysiological features correlated with the maturation of the organoid.[48] Since the quality of the extracellular signal recording with MEAs strongly depends on the interface of the cells to the electrodes, the functionalization of the electrode tips with nanoscale 3D structures has been extensively investigated.[49-51] However, these type of MEAs are still intended for use with 2D cell cultures and are limited in their possibilities to capture localized signals within deeper cell layers. Thus, the emergence of 3D culture architectures calls for 3D MEA systems.[52] Recent effort enabled highly elaborate, multifunctional 3D MEAs equipped with electrical, optical, chemical, and thermal interfaces to record and stimulate inner or superficial activities of 3D neural tissues, which in turn require complex and demanding fabrication protocols.[53, 54] A simpler approach is the functionalization of MEAs with 3D needle electrodes that can penetrate into the 3D cell cultures, closing the distance of the cell-electrode interface.[55] Here, classical photolithographic fabrication methods are restricted in their use, since, for example, the production of high-aspect-ratio needle structures is challenging and commonly subtractive etching processes have to be employed.[31, 55-58] This complicates the fabrication of needle electrodes with varying height, which would be beneficial to capture signals in different penetration depths into the cellular 3D architectures on a single MEA. As an alternative to the classical, clean-room-based production, additive manufacturing such as inkjet- and aerosol-jet printing strike a possible solution. In these direct-writing techniques, a fast 3D patterning of functional inks in high-aspect ratios and varying heights is easily achieved, which gives new possibilities for MEA designs.[59-61]

Previously, we have developed electrode arrays based on a conductive-polymer ink that feature µ-needle electrodes.[61] The µ-needle electrodes were built by aerosol-jet printing, which allowed processing inks with a high viscosity and a high material load dispersed in the ink, and was thus advantageous for a rapid yet controlled buildup of µ-needle electrodes in a point-wise printing approach. Conductive feedlines were made by ink-jet printing, which was suitable for printing

flat electrode structures in a time- and cost-effective manner. Here, this method was improved for printing µ-needle electrodes with significantly higher aspect ratios. The electrochemical properties and the long-term stability of the electrodes were assessed with cyclic voltammetry and impedance spectroscopy to measure the capacitance and impedance per µ-needle, respectively. Furthermore, the developed µ-needle electrode arrays (MnEAs) were successfully applied for electrophysiological measurements on 3D neural networks derived from hiPSCs. Firstly, we have employed an array of interconnected neurospheroids, which were spontaneously formed in a micro-honeycomb nest covered with gelatin nanofiber scaffolds.[62] Secondly, the measurements were performed on cerebral organoids placed on the MnEA. In both configurations, extracellular potentials were successfully recorded, confirming the functionality of the MnEA for neuronal activity measurements in 3D configurations.

2. Experimental section

Reagents were purchased from Sigma-Aldrich unless otherwise specified.

2.1. Preparation of PEDOT:PSS-MWCNT Ink. Carboxymethyl cellulose was dissolved at 0.025% (w/w) in a mixture of ethylene glycol and deionized water (3:1 w/w). Next, 0.4% (w/w) poly(3,4-ethylenedioxythiophene) poly(styrene sulfonate) (PEDOT:PSS) dry pellets were added, prior to homogenization with an ultrasonic horn for 1 min (127.5 µm amplitude, 6 mm KE76 probe, HD 2200.2, Bandelin). Subsequently, 0.1% (v/v) (3-glycidyloxypropyl)trimethoxysilane (GOPS), 0.01% (v/v) Dynol^{TM} 604 (Evonik), and 0.375% (w/w) carboxylated multiwalled carbon nanotubes (MWCNTs, ≥95 %, OD 15 nm, length 1-2 µm, IoLiTec Ionic Liquids Technologies) were added, and the ink was further sonicated for 10 min while cooling in an ice bath to avoid overheating. The PEDOT:PSS-MWCNT dispersion was centrifuged to remove large aggregates (ROTANTA 460 R, 10 min at 100 rcf) and the supernatant was used for printing.

2.2. Fabrication of µ-needle Electrode Arrays (MnEA). Commercial PEDOT:PSS inkjet ink (Orgacon IJ-1005, Agfa, Mortsel, Belgium) was modified by adding 0.2% (v/v) GOPS and 0.02% (v/v) Dynol 604 for increasing its surface wettability and stability in water. After a filtering step (0.2 µm PFDV filter), the modified ink was used to print thin conductive feedlines at the central area of the MEA in 6 layers by a state-of-the-art inkjet-printing system (F-series, Ceradrop) with disposable printing cartridges (DMC 1 pL, Fujifilm Dimatix) onto a polyethylene naphthalate (PEN) substrate, Teonex® Q65HA (DuPont Teijin Films), at 1 kHz jetting frequency and a drop spacing of 20 µm. During the printing process, the nozzle plate was kept at 24 °C and the substrate holder was kept at 37 °C. The substrates were dried at room temperature and the outer feedlines and contact pads were printed with a silver nanoparticle ink (Orgacon SI-J20x, Agfa) using 1 pL printing cartridges, a drop spacing of 20 µm, raster overlap of 50 µm, and jetting frequencies of 250 Hz and 1 kHz. The substrate holder and nozzle plate were both kept at 50 °C. After drying at 60 °C, µ-needles were aerosol-jet printed (Optomec) onto the tips of the feedlines using the PEDOT:PSS-MWCNT ink. Our system uses a pneumatic atomizer and a pre-humidified nitrogen gas stream. The µ-needles were fabricated with a push flow of 15 sccm (standard cubic centimeter per minute), a focusing ratio of 1, and a 150 µm nozzle. During printing, the temperature of the substrate holder was set to 60 °C. The µ-needles were printed by focusing the aerosol stream at a fixed position for 120, 150, 240, or 300 s. In addition, µ-needles were aerosol-jet printed with print durations of 60, 120, 240, and 300 s onto a gold-covered wafer for characterization by scanning electron microscopy (SEM). After printing the µ-needles, the silver feedlines were sintered and the solvents of the ink were evaporated at 150 °C overnight. The substrates were then plasma treated (O_2, 0.5 mbar, 190 W, 12 s, Diener Femto, Diener electronic) and passivated by inkjet printing a series of layers with UV curable insulator inks at 1 kHz jetting frequency, while nozzle plate and substrate-holder temperature was kept at 55 °C. For passivating the MnEA (see Figure 1A and 1B for the layout),

first, a discontinuous layer was printed with the commercial insulator ink DM-IN-7003-I (Dycotec Materials) with a splat spacing of 100 µm and UV-cured with a dose of approximately 0.25 J·cm^{-2}. Second, a ring layer was printed, which only covered the areas with the silver feedlines (splat spacing 30 µm, raster overlap 80 µm). Third, a continuous layer was printed with a splat spacing of 40 µm and a raster overlap 60 µm to cover the final passivated area on the MnEA. The printed passivation was UV cured with a dose of approximately 1 J·cm^{-2}. The height of needles printed with different duration times was measured using a laser scanning microscope (VK-X250, Keyence) before and after passivation and evaluated with MultiFileAnalyzer (Keyence).

2.3. Electrochemical Characterization. Conductivity of the PEDOT:PSS-MWCNT ink was measured on electrodes with contact pads, formed on glass substrates by drop-casting and molding using polyimide tapes (Figure S1). A voltage ramp, 5 mV·s^{-1}, was applied from -0.25 to 0.25 V using a potentiostat (VSP-300, BioLogic Science Instruments) and the current was recorded in a four-point configuration to assess the resistance R. The length l of the conductor track was measured using a caliper, the cross-sectional area A was measured with the laser scanning microscope (VK-X250, Keyence) and evaluated with MultiFileAnalyzer (Keyence). The conductivity σ was then calculated using the relation $\sigma = l/(A \cdot R)$.

Cyclic voltammetry (CV) was carried out on a final MnEA in phosphate-buffered saline (PBS) electrolyte, using the potentiostat (VSP-300, BioLogic Science Instruments) in a three-electrode configuration with a platinum-wire counter electrode and an Ag/AgCl reference electrode (3 M NaCl, RE-6, BASi). Electrochemical impedance spectroscopy (EIS) was performed using a PGSTAT20 potentiostat (Metrohm Autolab) in a three-electrode configuration with an Ag/AgCl reference electrode (3 M NaCl, RE-6, BASi). The data was recorded with EC-Lab (BioLogic Science Instruments) and FRA (Metrohm Autolab), and analyzed with MATLAB® (MathWorks).

2.4. Formation of Interconnected Neurospheroids on a Micro-honeycomb support.

Interconnected and active neurospheroids derived from hiPSCs were spontaneously formed on a micro-honeycomb substrate with gelatin nanofiber membranes we have developed previously.[62] Briefly, a 150 μm-thick, 9 mm-diameter micro-honeycomb disc surrounded by a 300 μm-thick support ring with an outer diameter of 13 mm was made in OrmoStamp photoresist (micro resist technology) by photolithography and soft lithography. The side-to-side distance of hexagonal holes of the micro-honeycomb and the frame width were 200 μm and 50 μm, respectively. Gelatin nanofibers were electrospun on the both sides of the micro-honeycomb substrate, which were coated with a 10 nm-thick gold layer by a metal sputter (K6785X, Emitech), similarly to our previous works.[62-64] Gelatin from porcine skin was dissolved at 15% (w/v) in a 10:14:21 (v/v) mixture of Milli-Q water, ethyl acetate, and acetic acid, and electrospun at 0.2 $mL \cdot h^{-1}$ from a syringe needle onto the substrate placed on a collector, at a distance of 10 cm under a bias voltage of 11 kV. Subsequently, the gelatin nanofiber mesh layers were crosslinked with 0.2 M 1-ethyl-3-(3-dimethylaminopropyl) carbodiimide hydrochloride and 0.2 M N-hydroxysuccinimide in ethanol for 4 h at room temperature, rinsed with ethanol, and dried.

hiPSCs (episomal line, Life Technologies) were cultured in Essential 8 Flex Medium (E8FM, Thermo Fisher Scientific) at 37 °C and 5% CO_2 in a humidified incubator, in a tissue culture dish treated with 5 $\mu g \cdot mL^{-1}$ vitronectin (VTN-N, Thermo Fisher Scientific) in PBS for 1 h at 37 °C. The hiPSCs were subsequently differentiated into neural precursor cells (NPCs) by following the protocol described elsewhere with a slight modification.[65] Dissociated hiPSCs were allowed to form embryoid bodies (EBs) in an ultra-low attachment round bottom 96-well plate (Corning) in E8FM for 2 days. The medium was replaced with neural induction medium (NIMa) composed of 1:1 mixture of Dulbecco's modified Eagle's medium and Ham's F-12 nutrient mix (DMEM/F-12), 1% (v/v) N2 supplement, 100 $U \cdot mL^{-1}$ penicillin−streptomycin

(PS) (all from Thermo Fisher Scientific), and 2 $\mu g \cdot mL^{-1}$ heparin (Stemcell Technologies). After 4 days of culture in NIMa, EBs were transferred on a tissue culture plate treated with 20 $\mu g \cdot mL^{-1}$ laminin in PBS for 1 h at 37 °C, and further cultured in NIMa for 7 days to generate pre-NPCs. Pre-NPCs were then cultured in neural precursor medium (NPM) composed of DMEM/F12 supplemented with 1% (v/v) N2, 2% (v/v) B27 minus vitamin A (Thermo Fisher Scientific), 1 $\mu g \cdot mL^{-1}$ laminin, 20 $ng \cdot mL^{-1}$ basic fibroblast growth factor (Stemcell Technologies), and 100 $U \cdot mL^{-1}$ PS. The medium was renewed every other day, and cells were subcultured in a dish treated with 1% (v/v) Geltrex (LDEV-free, reduced growth factor, Thermo Fisher Scientific) in DMEM/F-12 medium for 1 h at 37 °C. After five passages, cells were considered as NPCs and cryopreserved when necessary.

After being plasma treated (air plasma, Harrick PDC-002 equipped with a PDC-FMG PlasmaFlo) at ca. 70 Pa for 2 min and sterilized, the micro-honeycomb scaffold, covered with two separate layers of gelatin nanofiber mesh, was treated with 100 $\mu g \cdot mL^{-1}$ poly-L-ornithine at 4 °C overnight then 1% Geltrex in DMEM/F12 for 1 h at 37 °C in a humidified incubator. 3.0×10^5 NPCs were seeded on the flat side of the scaffold, allowed to adhere on the substrate for 2 h, and cultured in 1 mL of NPM for one day, prior to the same operation on the other side of the scaffold. The cells were further differentiated in neural differentiation medium (NDM) composed of neurobasal medium (Thermo Fisher Scientific) supplemented with 1% (v/v) N2, 2% (v/v) B27 minus vitamin A, 20 $ng \cdot mL^{-1}$ brain-derived neurotrophic factor and 20 $ng \cdot mL^{-1}$ glial cell-derived neurotrophic factor (both from Stemcell Technologies), 100 $U \cdot mL^{-1}$ PS, 1% (v/v) minimum essential medium non-essential amino acids (MEM-NEAA, Thermo Fisher Scientific), 1 μM dibutyryl cyclic adenosine monophosphate, and 2 $\mu g \cdot mL^{-1}$ laminin. NDM was fully renewed every other day for 4 weeks, and half the volume was renewed onward. Once the neural clusters were spontaneously formed and matured, the scaffold was used for electrophysiological measurements with MnEA, after 140 days of differentiation.

2.5. hiPSC Differentiation into Cerebral Organoids. Cerebral organoids were derived from hiPSCs by following the protocol of M. Lancaster, *et al.*,[15, 66] with a slight modification. Besides the non-fluorescent hiPSC line, hiPSCs expressing RFP-conjugated β-actin from Sigma-Aldrich (IPSC1028) were used. hiPSCs were cultured in Essential 8 Medium (E8M, Thermo Fisher Scientific) or E8FM. First, dissociated hiPSCs were seeded in an ultra-low attachment v-bottom 96-well plate (Greiner Bio-One) at a density of $4 \cdot 10^3$ or $6 \cdot 10^3$ cells per well in E8M with 10 µM ROCK inhibitor Y-27632 (Hello Bio). 24 h later, a half of the medium was replaced with E8M without ROCK inhibitor, and EBs were grown for 5 more days with medium changes every day in the same manner. On day 6, the EBs were transferred to a 35 mm non-adherent dish (Greiner Bio-One) and the medium was switched to neural induction medium (NIMb) composed of DMEM/F-12 supplemented with 1% (v/v) N2, 1% (v/v) Glutamax (Thermo Fisher Scientific), 1% (v/v) MEM-NEAA, 2 $\mu g \cdot mL^{-1}$ heparin, and 100 $U \cdot mL^{-1}$ PS, in which cells were cultured for 7 days to form neuroepithelium. On day 11, two days before switching to a maturation medium, the EBs were either individually embedded in 20 µL Matrigel (Corning), or 2% (v/v) Geltrex was added to the medium. On day 13, the medium was switched to maturation medium (MMa), composed of a 1:1 mixture of DMEM/F-12 and Neurobasal (Thermo Fisher Scientific), supplemented with 0.5% (v/v) N2, 2% (v/v) B27 minus vitamin A supplement (Thermo Fisher Scientific), 2.4 - 2.9 $\mu g \cdot mL^{-1}$ insulin, 50 µM 2-mercaptoethanol, 1% (v/v) Glutamax, 0.5% (v/v) MEM-NEAA, and 100 $U \cdot mL^{-1}$ PS, in which the EBs were cultured for 6 days with the addition of 3 µM CHIR99021 for the first two days. From day 20 onward, the organoids were cultured in MMb, which was MMa with B27 plus vitamin A supplement (Thermo Fisher Scientific) instead of B27 minus vitamin A supplement, and with the addition of 12.5 mM N-2-hydroxyethylpiperazine-N-2-ethane sulfonic acid (HEPES, Thermo Fisher Scientific) and 400 µM ascorbic acid. The medium was renewed twice per week. The timeline of hiPSC differentiation into cerebral organoids is summarized in Figure S2.

2.6. MnEA Recording on Neurospheroids and Cerebral Organoids. A 3 cm-diameter glass ring was attached to the MnEA with polydimethylsiloxane (PDMS, RTV 615 kit, Momentive) as a reservoir for the culture medium. Prior to use, the MnEA was incubated with 0.01% (w/v) poly-L-ornithine solution at room temperature for 1 h, rinsed with isopropanol, and dried under UV irradiation for 1 h. The micro-honeycomb support with interconnected neurospheroids, after 140d of differentiation, was positioned onto the MnEA and held in place with a PDMS ring (see Figure 3A). For cerebral organoids, a 400 µm-thick support with four 2.5 mm-diameter wells made of OrmoStamp was attached to the MnEA to hold the organoids. After 60 d of differentiation, an organoid was placed in each well, where an array of 12 µ-needle electrodes were positioned (see Figure 1A, 4B, and 4D). The medium underneath the organoids was carefully aspirated to improve the contact between the organoids and electrodes. A disc of gelled Matrigel was gently placed to cover the organoids to press them down against the electrodes and fixed further with additional Matrigel by incubating at 37 °C for 25 min. Once the micro-honeycomb support or cerebral organoids were placed on the MnEA, 3 mL of NDM or MMb, respectively, was added in the glass ring chamber. Extracellular signals were observed with a MEA2100-Mini amplification system (Multi Channel Systems) and a sampling rate of 10 or 40 kHz. The MnEA was inserted into the amplifier head stage and the glass ring chamber was closed with a custom PDMS cap to avoid contamination during the measurement. The medium bath was grounded with an Ag/AgCl reference electrode (3M NaCl, RE-6, BASi) that was soaked in 100 $U \cdot mL^{-1}$ PS in PBS for 30 min before insertion through a hole in the PDMS cap. During the measurement, the headstage of the amplifier system with the MnEA was kept at 37 °C in 5 % CO_2 atmosphere in a humidified incubator, with the medium being changed twice per week. Measurements on cerebral organoids were made also with a commercial 2D MEA (60MEA200/30iR-Ti-gr, Multi Channel Systems), where an organoid was placed on the 2D electrodes with ca. 200 µL of MMb to cover all the electrodes, including the integrated

reference electrode. Data was recorded using a bandpass filter between 10 mHz and 4 kHz. The signal analyses were performed in MATLAB (MathWorks). Spikes in the trace were detected by setting an amplitude threshold *Thr* as a measure of an estimate of the background noise ξ, $Thr = 5 \cdot \xi$, where ξ is the median absolute deviation of the signal in unit of V divided by the constant scale factor 0.6745, i.e., $\xi = \text{median}(|Signal|)/0.6745$. The factor is reciprocal of the quantile function of the standard normal distribution at a probability of 75%, i.e., $\sqrt{2}erf^{-1}(0.5) = 0.6745$, which denotes an estimation of the standard deviation of the data with diminished interference by the spikes.[67, 68]

2.7. Cryosectioning and Immunofluorescence Staining of Cerebral Organoids.

The preparation and cryosectioning of the organoids were performed based on literature.[69, 70] After being rinsed with PBS briefly, the organoid was incubated in 1 mL 4% (w/v) paraformaldehyde (Thermo Fisher Scientific) in PBS at 4 °C overnight with agitation. The organoid was rinsed 3 times in 1 mL PBS for 10 min with agitation at room temperature, prior to be soaked in 2 mL of 30% (w/v) sucrose in PBS for 3 d at 4 °C until the organoid sedimented. Next, the organoid was placed in an inclusion mold (Simport) and the sucrose solution was carefully removed. Subsequently, the mold was filled with Neg-50 frozen section medium (Richard-Allan Scientific), immersed gradually in 2-methybutane at -75 °C for 2 min on dry ice under a fume hood, and kept at -80 °C until cryosectioning.

For cryosectioning, the frozen block was removed from the mold and mounted with Neg-50 on a sample holder silver disk inside a CM3050S cryostat (Leica Biosystems) at -20 °C for slicing. The block was sectioned into 20 µm-thick slices that were transferred on a Superfrost Plus microscope slide (Thermo Fisher Scientific). The slide was stored at -80 °C.

Before immunofluorescence staining, the slide was let at room temperature for 30 min prior to rehydrating with PBS for 5 min. After removal of PBS and demarcation with PAP Pen (Kisker Biotech) around the organoid slices, the slide was put in a humidified chamber and

approximately 200 µL of permeabilization/blocking (PB) solution, composed of 0.1% (v/v) Triton X-100 and 3% (w/v) bovine serum albumin in PBS, was placed on the sample and incubated for 1 h at room temperature. After removing PB solution, the slide was incubated with primary antibodies, anti-Sox2 (Invitrogen, PA1-094X, 1:500 dilution in PB solution) and anti-Tau (T9450, 1:500), in the humidified chamber at 4 °C overnight. The slide was then rinsed 3 times with PBS by 10 min incubation before adding the secondary antibodies, Alexa Fluor 488 anti-mouse antibody (Invitrogen, A-1101, 1:100) and Alexa Fluor 555 anti-rabbit antibody (Invitrogen, A-31572, 1:100), and 2 $\mu g \cdot mL^{-1}$ Hoechst 33342 in PB solution. The slide was protected from light and incubated for 1 h at room temperature in the humidified chamber. Next, the slide was rinsed 3 times with PBS and dried briefly before being covered with Immu-Mount (Epredia) and a cover slide ($24 \cdot 50\ mm^2$), and sealed with nail polish. The slide was stored at -20 °C.

2.8. Imaging. Phase contrast and epifluorescence images were taken with a DMi1 microscope equipped with a LC170 camera and a DM IL LED microscope equipped with a K3M camera, respectively (Leica Microsystems). An LSM 900 (Zeiss) was employed to obtain confocal microscopy images. SEM images were taken by NVision 40 (Zeiss).

3 Results and Discussion

3.1 High-aspect Ratio µ-needle Electrode Arrays (MnEAs). We combine inkjet and aerosol-jet printing to fabricate our MnEAs similarly as shown in our previous work.[61] Here, the ink for the aerosol-jet printing has been improved by a two-fold increase of the ratio of the conductive components (PEDOT:PSS- and MWCNT-phase) to the passivating components (CMC- and GOPS-phase) necessary for adhesion and stability in aqueous electrolytes, and by modifying the ink solvent to decrease the viscosity of the ink for an improved atomization process. The novel ink composition allowed an extended printing duration without clogging the atomizer

nozzle and a more precise control of the needle height by modulation of the print duration. The overall production of the devices involved three main steps: i) inkjet printing of conductive feedlines in commercial PEDOT:PSS and silver nanoparticle-based inks onto a flexible PEN substrate, ii) aerosol-jet printing of the µ-needles onto the electrode tips using a custom-made PEDOT:PSS-MWCNT composite ink, and iii) inkjet printing of a commercial UV curable polyacrylate-based ink as insulation. The layout and a finished MnEA is shown in Figure 1A and 1B, respectively. Each chip contained a total of 48 electrodes, arranged in 4 separate areas of 12 electrodes each, with a needle pitch of 250 µm in x- and y-direction. A microscope image of a MnEA without passivation is shown in Figure 1C. It is worth noted that the pitch of the µ-needle electrodes can be decreased down to ca. 100 µm, which is limited rather by the width of the ink-jet printed traces, while the diameter of a single needle electrode is in the range of 20 µm. Higher electrode densities could be achieved using different processes for trace patterning, such as lithography or laser ablation.

The inner PEDOT:PSS feedlines at the central chip areas are beneficial for minimizing potential cytotoxic effects originating from diffusing silver nanoparticles through the porous µ-needles and, due to their transparency, for observation of the cells. To print the µ-needles onto the tips of the PEDOT:PSS feedlines, the PEDOT:PSS-MWCNT aerosol stream was focused onto the desired position for 120 s, 240 s, or 150/300 s depending on the desired final needle height. Figure 1D shows a SEM image of needles fabricated with increasing print durations ranging from 60 s to 300 s and demonstrates the control of the needle height in the point-wise printing process. A close-up SEM image in Figure 1E verifies the presence of the MWCNTs in the deposited structures. The print parameters of the dielectric passivation layer were adjusted so that the passivating film was significantly lower than the height of the needles. Therefore, the needles protruded through the liquid dielectric layer were not covered. The average diameter and height of the uncovered part, i.e., above the passivation layer, of µ-needle electrodes printed

with a duration of 240 s was measured to be 19 ± 2 µm and 158 ± 13 µm, respectively (aspect ratio of 8.5 ± 1.1, n = 12 electrodes; mean ± standard deviation). In the approximation of a cylindrical shape, the surface area and volume of the uncovered µ-needles are calculated to be $(10 \pm 2)\cdot 10^3$ µm² and $(44 \pm 12)\cdot 10^3$ µm³, respectively. Furthermore, MnEAs were printed with alternating needle heights with print durations of 150 s and 300 s, which resulted in uncovered needle height of 60 ± 20 µm and 185 ± 26 µm, respectively. The measured dimensions of the µ-needle electrodes fabricated with different printing durations and the passivation layer on a finished MnEA were illustrated in Figure 1F.

3.2 Characterization of the µ-needle Electrode Arrays. Conductivity of the PEDOT:PSS-MWCNT ink was measured on a simplified electrode configuration (Figure S1). The measured average conductivity σ was $(5.9 \pm 3.6) \cdot 10^3$ S·m^{-1} (n = 14), which is significantly higher compared to our previous work.[61] Next, CV was carried out on a final µ-needle electrode array with needles with an average height of 158 ± 13 µm in phosphate-buffered saline electrolyte. The cyclic voltammograms were recorded by sweeping the working electrode potential between 0 V and 0.6 V versus the Ag/AgCl reference electrode with different scan rates of 10, 50, 100, and 200 mV·s^{-1} for 10 cycles. Figure 2A shows the results of a representative measurement. The capacitance *C* of the µ-needle electrodes was calculated for different scan rates *s* from the measured anodic and cathodic currents (i_a and i_c, respectively) with the relation $C = (i_a - i_c)/2s$ at a working electrode potential of 0.3 V. For higher scan rates (>10 mV·s^{-1}) the porous material exhibited a decreased specific volumetric capacitance for increasing scan rates as shown in Figure 2B. The maximum and minimum volumetric capacitance for scan rates of 10 mV·s^{-1} and 200 mV·s^{-1} were calculated to be 50 ± 15 F·cm^{-3} and 20 ± 5 F·cm^{-3} (n = 11 electrodes, mean ± standard deviation), respectively, which are comparable to results for PEDOT:PSS reported in literature.[71] The measurements were performed for a total of 12

electrodes, while one electrode showed a significantly smaller capacitance by one order of magnitude and was therefore considered to be non-functional and excluded from analysis.

For further characterization of the performance of the µ-needle electrodes, EIS was performed. A sine signal of low-amplitude (40 mV peak-to-peak) was applied with a frequency from 1 Hz to 1 MHz. The recorded impedance and phase curves (example given in Figure 2C) showed the typical response for a combination of several *RC* elements, as expected for porous composite materials with internally distributed contact impedances (Figure 2C). Nineteen out of 21 electrodes were functional (yield of 90%, 2 electrodes had a significantly higher impedance). For testing the long-term stability under cell-culture conditions, the impedance of the electrodes at 1 kHz was measured after incubation in salt solution at 37 °C for up to 42 days (d) (Figure 2D). Initially, the electrodes showed a resistive behavior at 1 kHz (phase angle of 5° ± 4 °) with an impedance of 8.1 ± 4.4 kΩ (n = 19, µ-needles with an average height of 158 ± 13 µm). After 14 d, all 19 of the initially functional electrodes remained functional and the impedance did change only slightly to to 7.2 ± 2.0 kΩ (n = 19).

3.3 MnEA Recording of Neuronal Activity on hiPSC-Derived Neurospheroids. First, the MnEAs were applied to the hiPSC-derived interconnected neurospheroids, spontaneously formed on the micro-honeycomb substrate. As we reported previously,[62] this self-organized 3D structure provides an active network of neurons and glia, with inter-neuron synaptic connections and signal propagation over the substrate. Before the MnEA measurement, we have confirmed the neural activity of a neurospheroid network on another micro-honeycomb substrate from the same culture by calcium imaging (data not shown). MnEAs with ca. 185 µm and 60 µm-high needles were used for the detection of neuronal activities as extracellular signals from the neurospheroids after 140 d of differentiation. As shown in Figure 3A, the substrate was integrated onto the MnEA and held in place by a PDMS ring. Due to the mismatch between the layout of the electrodes and the micro-honeycomb, µ-needle electrodes either

penetrated the gelatin nanofiber layer and made contact with the neurospheroids, became broken, or became bent along the substrate and made contact with neurons covering the substrate surface (Figure S3). Signals were observed with the amplifier system using a sampling rate of 10 kHz and recorded on a maximum of 17 electrodes out of total 48 electrodes on the MnEA. The left panel of Figure 3B shows representative time traces of signals detected with μ-needle electrodes at different configurations as depicted in Figure 3A. The right panel of Figure 3B shows the average spike shapes in the traces with standard deviations (n = 119 (i), 213 (ii), 245 (iii), and 378 (iv)). In the configuration (i), a long μ-needle electrode from the group with an average height of 185 ± 26 μm was penetrating a compartment of micro-honeycomb substrate and in contact with a neurospheroid. Signal-to-noise ratio (SNR, peak amplitude/root mean square noise) was measured to be 8.0 ± 0.9 (standard deviation). In the second configuration, the long electrode was completely bent as shown in the image (ii) in the right panel of Figure 3A. Nonetheless, signals could be detected along the electrode that was in contact with the neurons at the bottom of the micro-honeycomb substrate. SNR was measured to be 6.7 ± 0.6. Similarly, signals were detected by shorter electrodes from the group with an average height of 60 ± 20 μm that were slightly bent and in contact with the neural network at the bottom of the substrate (iii), or in contact at its extremity with the neurons on the frame (iv). SNRs were measured to be 7.3 ± 0.7 and 7.7 ± 0.8, respectively. As shown in Figure 3B, both negative and positive peaks were observed, which we hypothesize is due to different positions of neurons, i.e., a perisomatic or a dendritic area, the μ-needle electrode was in contact with as described by Obien, *et al*.[72]

The extracellular signals from the 3D neural network were successfully recorded by the MnEA confirming the electrophysiological activity of the cells as demonstrated in our previous study by calcium imaging,[62] as well as the functionality of the MnEA. Unlike the calcium imaging that is harmful for cells, MnEA allows us to make long-term activity measurements. Moreover,

the robustness of the MnEA against deformation demonstrated here is advantageous when targeting a dense tissue.

3.4. MnEA Recording on hiPSC-Derived Cerebral Organoids.

Next, a more complex and *in vivo*-like neural architecture was targeted, which was achieved by forming cerebral organoids derived from hiPSCs. Figure 4A shows a photograph of representative organoids in culture with a diameter of ca. 3-5 mm. In this case, the MnEA was designed to make measurements on 4 organoids, each of them being immobilized on an array of 12 μ-needle electrodes (see Figure 1A) and supported by a 400 μm-deep, 2.5 mm-diameter well. MnEAs with approx. 158 μm high μ-needles were used for the detection of extracellular signals from cerebral organoids. As shown in Figure 4B, 4 organoids were immobilized on the MnEA, which was inserted in the headstage of the amplifier system. After being filled with medium, the glass ring chamber on the MnEA was sealed with a PDMS lid equipped with an Ag/AgCl reference electrode. A bright-field microscopy image of an organoid on the array of 12 μ-needle electrodes is shown in Figure 4C, where the edge of the well is indicated by a yellow arrowhead. To make the μ-needle electrodes penetrate into the organoids, the electrodes were dried to maintain their rigidity before the installation of the organoids. Since the organoids were highly deformable and fragile, after removal of culture medium around the organoids, they were gently pressed against the electrodes simply by the weight of a pre-formed Matrigel, and further immobilized by additional Matrigel solution, as depicted in Figure 4D. None of the μ-needle electrodes were broken or deformed due to insertion. To visualize the position of the organoid on the MnEA, cerebral organoids formed from hiPSCs expressing RFP-conjugated β-actin were set on the MnEA as described above, and observed by confocal microscopy. Figure 4E shows one of the obtained images focused on the conductive feedlines (center) with cross-sections across the blue and red lines on the x-y plane (top and right, respectively). The bottom of the organoid was successfully visualized, which is indicated with yellow arrowheads in the

cross-sectional images. Fluorescence signals were also observed at the surface of the PEN substrate, at the same z position as the conductive feedlines. The smallest and largest distance between the organoid bottom and the PEN substrate were 62.5 µm and 250.6 µm, respectively. The distance between the µ-needle electrode tip and the PEN substrate was deduced to be 218 ± 26 µm, given that the thickness of the passivation layer and the height of the exposed part of µ-needle were 60 ± 22 µm and 158 ± 13 µm, respectively. We thus conclude that the cerebral organoids were in good contact with several of the µ-needle electrodes. The extracellular signals were recorded with the amplifier system using a sampling rate of 40 kHz and a selected filter bandwidth of 10 mHz to 4 kHz. The system was kept at 37 °C in 5% CO_2 atmosphere in a humidified incubator during long-term measurements. Clear signals were obtained from up to 2 µ-needle electrodes per organoid. An example time trace and the average spike shape of the detected signals (n = 63) are shown in Figure 4F (i), while examples of individual spike shapes detected by spike sorting are shown in Figure S4. The signals were obtained from an organoid after 77 d of differentiation and had been placed on the MnEA for 13 d before recording started. As a comparison, we conducted measurements with a commercial 2D MEA on an organoid at day 63. The time trace and the average spike shape (n = 25) are shown in Figure 4F (ii). To confirm the successful formation of cerebral organoids, immunofluorescence analyses were performed in a separate experiment. As shown in Figure 4G, the organoid after 78 d of differentiation exhibited a self-organized architecture seen well with DNA staining (Hoechst, blue), and the presence of neural progenitors (Sox2, magenta) forming rosette-like structures and neurons (Tau, cyan) at the periphery of the organoid.

As described above, we have successfully obtained extracellular signals from cerebral organoids both with the 3D MnEA and with the commercial 2D MEA. While the signals recorded with the 2D MEA have similar characteristics of peak heights and widths compared to the results with the neurospheroid network, typically temporally broadened signals were

recorded by the MnEA. This in part can be due to the difference of the number of neurons in contact with the electrodes. The commercial 2D MEA has 30 µm-diameter flat electrodes with a 200 µm spacing, whereas the exposed part of the µ-needle electrode of the MnEA with a diameter of 19 ± 2 µm and a height of 158 ± 13 µm is entirely conductive, having 51 times larger conductive area per electrode than the 2D MEA. We hypothesize that the peaks we recorded from the neurospheroid network with the MnEA and from the cerebral organoid with the 2D MEA originate from single neurons in contact with the electrode. On the other hand, the peaks recorded from the cerebral organoid with the MnEA seem to be superimposed signals from multiple sources. Despite the long period of measurements with the MnEA, no synchronized activity was observed between different channels. It is also worth noting that the neurons tend to localize rather at the surface of the organoids at this stage, as seen in Figure 4G. To study the synchrony of neural activities in cerebral organoids, they can be placed on MnEA at a later stage to make measurements on more matured organoids and the medium for electrophysiological measurements can be optimized. Even though spike-sorting algorithms can be used to discern different recordings sites in the 3D culture, further research should be directed at developing suitable passivation methods for the production of selective electrode openings on the tip or along the shaft of the µ-needle electrodes.[73, 74] Locally confined signals could be obtained by varying the height and lateral position of the exposed electrodes within the array, e.g. using laser ablation. This would enable making selective measurements at targeted regions of the 3D architectures in the cerebral organoid.

With the versatile additive-manufacturing approach shown in this work, the MnEA can be tailored for simultaneously targeting specific regions on cerebral organoids or other 3D neural network assemblies in future studies. Further, the approach allows the MnEA design to be flexibly adapted to various microfluidic devices for a precise control of microenvironment,

paving a way towards brain-on-a-chip platforms for high-throughput investigations of electrophysiological activity in 3D neural tissues.

Conclusion

We have fabricated an array of high-aspect-ratio µ-needle electrodes by combining aerosol-jet printing of an optimized PEDOT:PSS-MWCNT ink, and inkjet printing of conductive feedlines and passivation layers. This µ-needle electrode array (MnEA) was successfully applied for electrophysiological signal recordings on two different 3D neural architectures, firstly on interconnected neurospheroids spontaneously organized on a micro-honeycomb substrate, and secondly on cerebral organoids, which were both differentiated from hiPSCs. The µ-needle electrodes were functional for at least 6 weeks under a physiological condition showing their applicability for long-term measurements. Furthermore, the high-aspect ratio of the electrodes produced via combined inkjet and aerosol-jet printing allows flexible designs and fast prototyping, thus opening a new paradigm of 3D microelectrode array development.

FIGURES

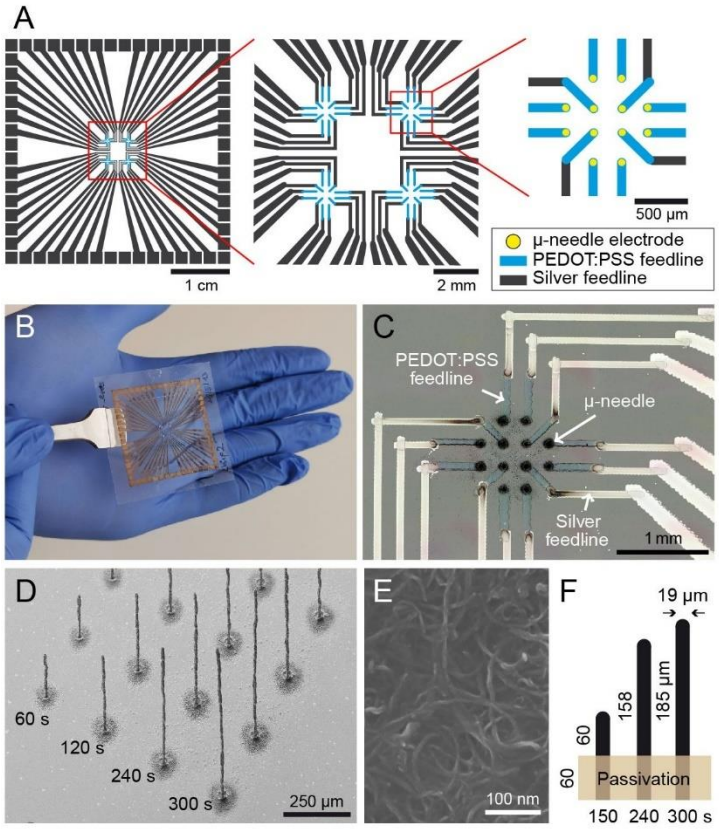

Figure 1. Aerosol-jet and inkjet-printed µ-needle electrode array (MnEA). (A) Layout of the MnEA indicating the positions of inkjet-printed silver (gray) and PEDOT:PSS (light blue) feedlines and aerosol-jet-printed µ-needle electrodes (yellow). (B) Photograph of a MnEA with µ-needles (average height of 158 ± 13 µm) used for the electrochemical measurements. (C) Bright-field microscopy image of a MnEA without passivation layer. The shape of µ-needles is invisible due to their orientation vertical to the substrate. (D) SEM image of a 4 by 4 grid of µ-needles printed in different heights with print durations ranging from 60-300 s onto a gold-covered wafer. (E) Close-up SEM image of MWCNTs at the surface of printed structures. (F) Schematic illustration of the measured dimensions of the µ-needle electrodes with different printing durations (150, 240, 300 s) and the passivation layer on a MnEA.

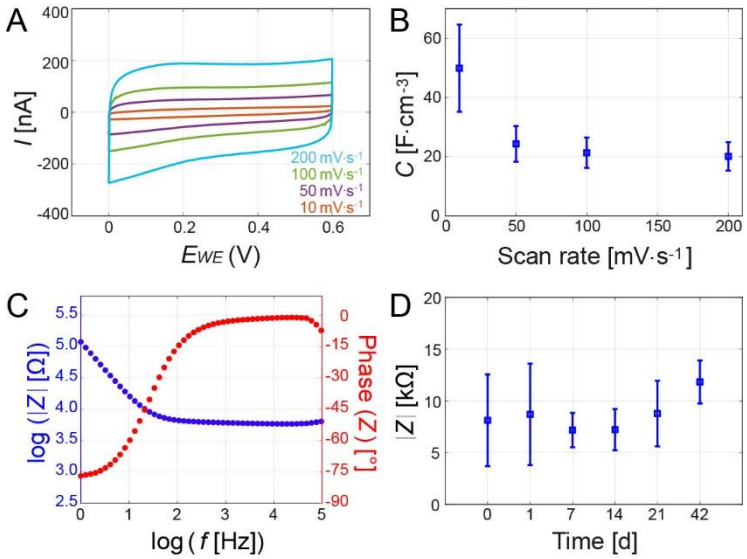

Figure 2. Electrochemical characterization of µ-needle electrodes. (A) Example cyclic voltammograms, i.e., current I plotted against the potential at the working electrode, for a µ-needle recorded with different scan rates of 10, 50, 100, and 200 $mV \cdot s^{-1}$. (B) Specific volumetric capacitance C for different scan rates (n = 11, ± standard deviation). (C) Example impedance |Z| and phase curves versus the applied frequency *f* on logarithmic scales. (D) Impedance |Z| at 1 kHz given after incubation in PBS at 37 °C in a humidified incubator for up to 14 d (n = 19, ± standard deviation), 21 d (n = 18), and 42 d (n = 17).

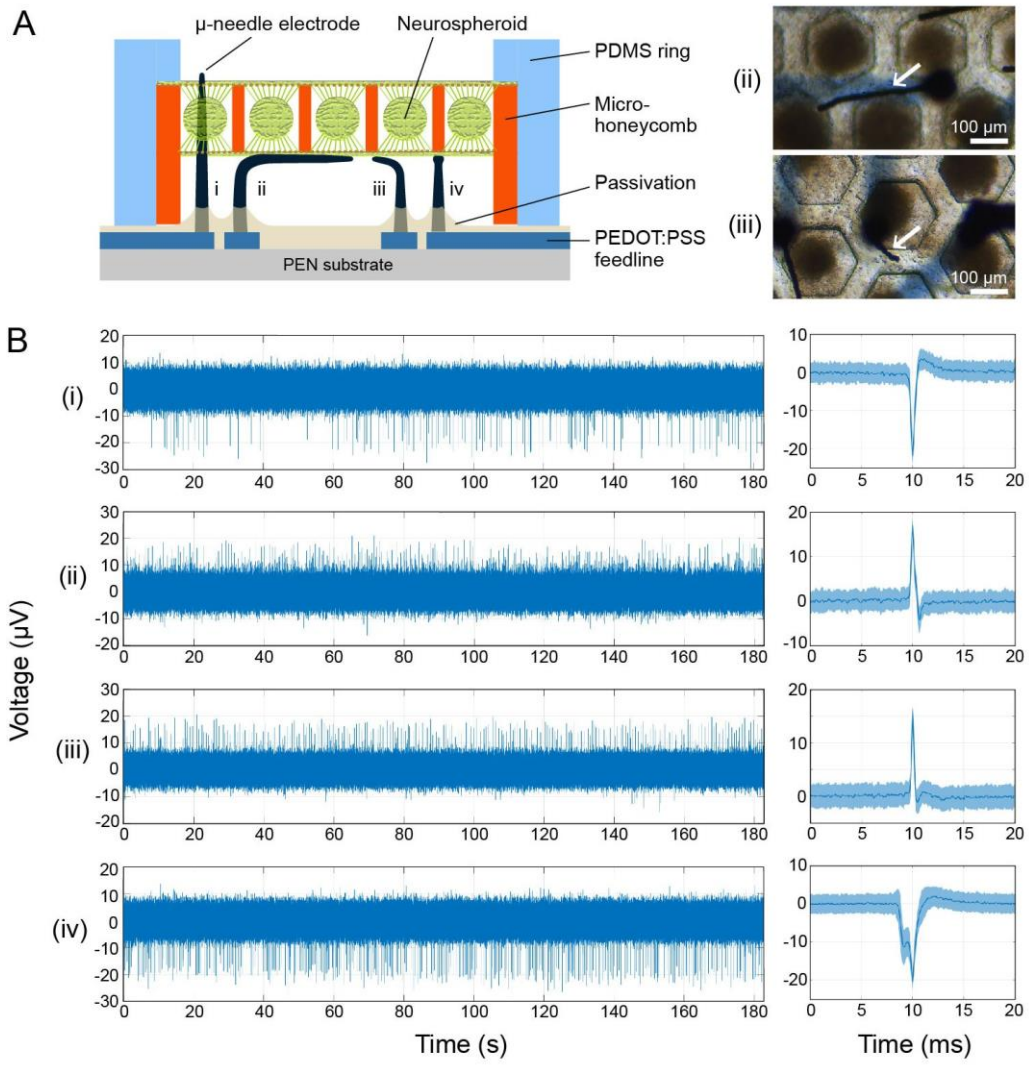

Figure 3. MnEA recording on hiPSC-derived, interconnected neurospheroids supported by a micro-honeycomb substrate. (A) Schematic illustration (left, not reflecting actual dimensions) and bright-field microscopy images (right) of the neurospheroids-laden micro-honeycomb substrate placed on the MnEA, depicting μ-needle electrodes at different configurations. μ-needles in the microscopy images are indicated with white arrows. (B) Time traces of signals detected with a μ-needle electrode from the group with an average height of 185 ± 26 μm penetrating a micro-honeycomb compartment (i), a bent μ-needle electrode from the group with an average height of 185 ± 26 μm (ii), a slightly bent μ-needle electrode from the group with an average height of 60 ± 20 μm (iii), and a μ-needle electrode from the group with an average

height of 60 ± 20 μm (iv) (left). Average shapes of the recorded spikes in the traces ± standard deviations (n = 119 (i), 213 (ii), 245 (iii), and 378 (iv), right). SNRs are 8.0 ± 0.9 (i), 6.7 ± 0.6 (ii), 7.3 ± 0.7 (iii), and 7.7 ± 0.8 (iv).

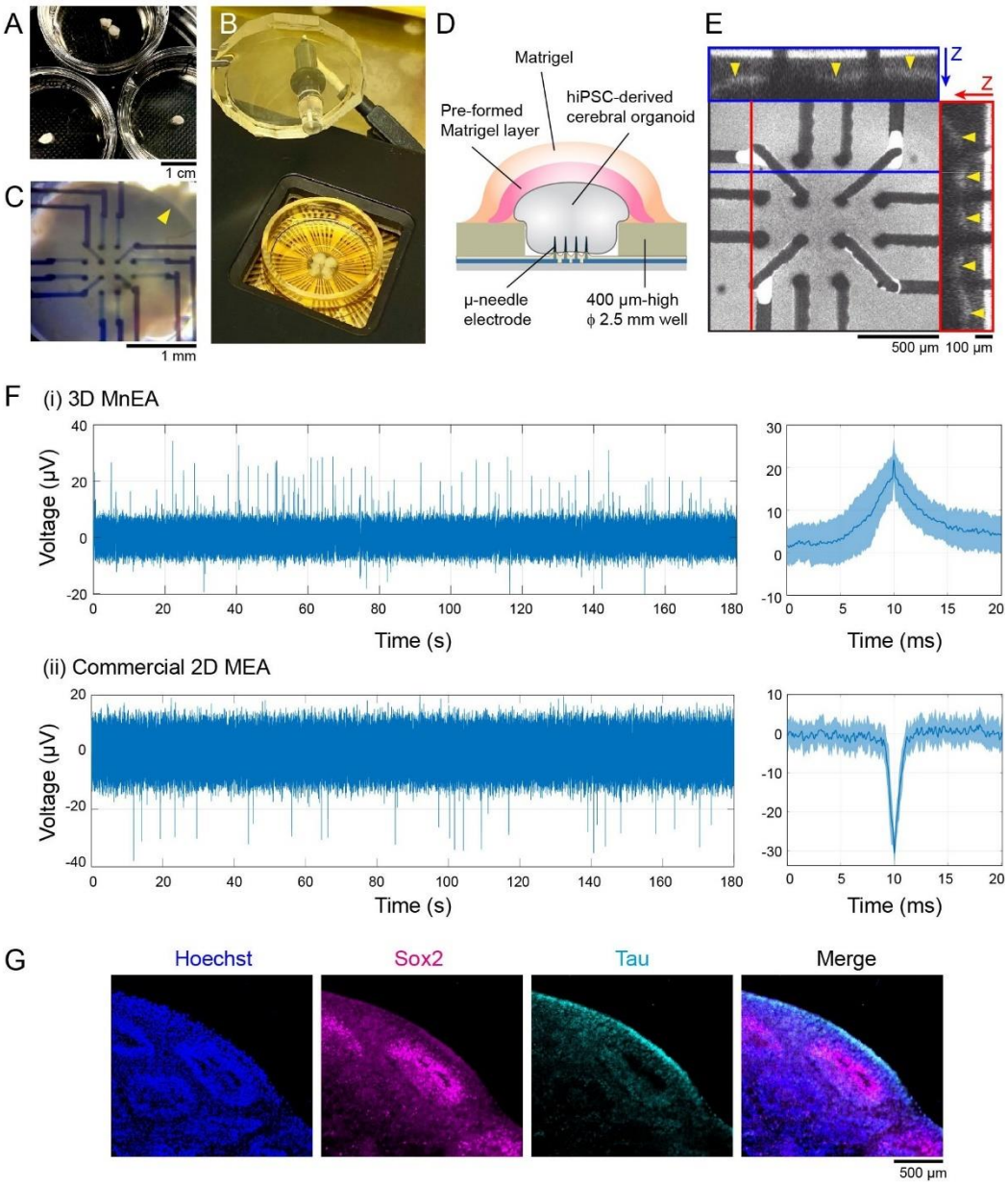

Figure 4. MnEA recording on hiPSC-derived cerebral organoids. (A) Photograph of cerebral organoids in culture before being installed on a MnEA. (B) Photograph of the experimental setup. Four organoids were immobilized in 4 wells on the MnEA, which was inserted in the headstage of the amplifier system. After being filled with medium, the glass ring chamber on the MnEA was sealed with a PDMS lid equipped with an Ag/AgCl reference electrode. (C) Bright-field microscopy image of an organoid on the array of 12 μ-needle electrodes. The edge of the well is indicated by a yellow arrowhead. (D) Schematic illustration depicting an organoid

placed in a well with 12 μ-needle electrodes on a MnEA. The scheme does not reflect actual dimensions. (E) Confocal microscopy image of an organoid derived from hiPSCs expressing RFP-conjugated β-actin placed on an array of 12 μ-needle electrodes on a MnEA. Top and right panel shows the cross-sectional image along the blue and the red line in the image in an x-y plane, respectively. The bottom of the organoid is indicated with yellow arrowheads. (F) Time traces of signals detected via a MnEA with μ-needle electrodes (average height of 158 ± 13 μm) from an organoid at day 77 (i), and via a commercial 2D MEA from an organoid an organoid at day 63 (ii) (left). Average shapes of the recorded spikes in the traces ± standard deviations (n = 63 (i), 25 (ii), right). SNRs are 8.5 ± 1.9 (i) and 7.7 ± 0.8 (ii). (G) Epifluorescence microscopy images of the immunofluorescence (Sox2, magenta; Tau, cyan) and Hoechst (blue) in a 20-μm thick section of a cerebral organoid after 78 d of differentiation.

ASSOCIATED CONTENT
Supporting Information. Figures S1-S4.

AUTHOR INFORMATION

Corresponding Author

*Yong Chen - PASTEUR, Département de Chimie, École Normale Supérieure, PSL University, Sorbonne Université, CNRS, 75005 Paris, France; orcid.org/0000-0002-2903-8753;

Email: yong.chen@ens.psl.eu

*Bernhard Wolfrum - Neuroelectronics, Munich Institute of Biomedical Engineering, Department of Electrical Engineering, Technical University of Munich, 85748 Garching, Germany; orcid.org/0000-0003-4438-3755

Email: bernhard.wolfrum@tum.de

*Ayako Yamada - PASTEUR, Département de Chimie, École Normale Supérieure, PSL University, Sorbonne Université, CNRS, 75005 Paris, France; orcid.org/ 0000-0003-3162-3318; Email: ayako.yamada@ens.psl.eu

Author Contributions

‡These authors contributed equally.

ACKNOWLEDGMENT

S. Z. and B. H. have been supported by TUM Graduate School and FGZ-EI Internationalization grant, and the Guangzhou Elite fellowship, respectively. This work was supported by the French National Research Agency ANR (ANR-19-CE18-0009, ANR-17-CE09-0017), Ils-de-France Region (DIM ELICIT), "Institut Pierre-Gilles de Gennes (IPGG)" (laboratoire d'excellence, "Investissements d'avenir" program ANR-10-IDEX-0001-02 PSL, ANR-10-LABX-31), by the Federal Ministry of Education and Research (BMBF) and the Free State of Bavaria under the Excellence Strategy of the Federal Government and the Länder through the ONE MUNICH Project Munich Multiscale Biofabrication. This work has benefited from the technical contribution of the joint service unit CNRS UAR 3750 (IPGG). The authors thank Andreas Offenhäusser (Forschungszentrum Jülich), Frédéric Darios, and Dominic Samaroo (ICM Institute for Brain and Spinal Cord) for fruitful discussions, and the histology platform of ICM Institute for Brain and Spinal Cord for the technical support.

REFERENCES

1. Mertens, J.; Marchetto, M. C.; Bardy, C.; Gage, F. H., Evaluating Cell Reprogramming, Differentiation and Conversion Technologies in Neuroscience. *Nat. Rev. Neurosci.* **2016,** *17*, 424-437.
2. Tukker, A. M.; Wijnolts, F. M. J.; de Groot, A.; Westerink, R. H. S., Human iPSC-Derived Neuronal Models for In Vitro Neurotoxicity Assessment. *Neurotoxicology* **2018,** *67*, 215-225.
3. Bieri, G.; Gitler, A. D.; Brahic, M., Internalization, Axonal Transport and Release of Fibrillar Forms of Alpha-Synuclein. *Neurobiol. Dis.* **2018,** *109*, 219-225.
4. Yi, Y.; Park, J.; Lim, J.; Lee, C. J.; Lee, S. H., Central Nervous System and its Disease Models on a Chip. *Trends Biotechnol.* **2015,** *33*, 762-776.
5. Holmes, T. C.; de Lacalle, S.; Su, X.; Liu, G.; Rich, A.; Zhang, S., Extensive Neurite Outgrowth and Active Synapse Formation on Self-Assembling Peptide Scaffolds. *Proc. Natl. Acad. Sci. U. S. A.* **2000,** *97*, 6728-6733.
6. Engler, A. J.; Sen, S.; Sweeney, H. L.; Discher, D. E., Matrix Elasticity Directs Stem Cell Lineage Specification. *Cell* **2006,** *126*, 677-689.

7. Yamada, K. M.; Cukierman, E., Modeling Tissue Morphogenesis and Cancer in 3D. *Cell* **2007,** *130*, 601-610.
8. Irons, H. R.; Cullen, D. K.; Shapiro, N. P.; Lambert, N. A.; Lee, R. H.; Laplaca, M. C., Three-Dimensional Neural Constructs: a Novel Platform for Neurophysiological Investigation. *J. Neural Eng.* **2008,** *5*, 333-341.
9. Teixeira, A. I.; Ilkhanizadeh, S.; Wigenius, J. A.; Duckworth, J. K.; Inganas, O.; Hermanson, O., The Promotion of Neuronal Maturation on Soft Substrates. *Biomater.* **2009,** *30*, 4567-4572.
10. Tibbitt, M. W.; Anseth, K. S., Dynamic Microenvironments: the Fourth Dimension. *Sci. Transl. Med.* **2012,** *4*, 160ps24.
11. Seidel, D.; Krinke, D.; Jahnke, H. G.; Hirche, A.; Kloss, D.; Mack, T. G.; Striggow, F.; Robitzki, A., Induced Tauopathy in a Novel 3D-Culture Model Mediates Neurodegenerative Processes: a Real-Time Study on Biochips. *PLoS One* **2012,** *7*, e49150.
12. Franze, K.; Janmey, P. A.; Guck, J., Mechanics in Neuronal Development and Repair. *Annu. Rev. Biomed. Eng.* **2013,** *15*, 227-251.
13. Zhang, D.; Pekkanen-Mattila, M.; Shahsavani, M.; Falk, A.; Teixeira, A. I.; Herland, A., A 3D Alzheimer's Disease Culture Model and the Induction of P21-Activated Kinase Mediated Sensing in iPSC Derived Neurons. *Biomater.* **2014,** *35*, 1420-1428.
14. Park, J.; Lee, B. K.; Jeong, G. S.; Hyun, J. K.; Lee, C. J.; Lee, S. H., Three-Dimensional Brain-on-a-Chip with an Interstitial Level of Flow and its Application as an In Vitro Model of Alzheimer's Disease. *Lab Chip* **2015,** *15*, 141-150.
15. Lancaster, M. A.; Renner, M.; Martin, C. A.; Wenzel, D.; Bicknell, L. S.; Hurles, M. E.; Homfray, T.; Penninger, J. M.; Jackson, A. P.; Knoblich, J. A., Cerebral Organoids Model Human Brain Development and Microcephaly. *Nature* **2013,** *501*, 373-379.
16. Choi, Y. J.; Park, J.; Lee, S. H., Size-Controllable Networked Neurospheres as a 3D Neuronal Tissue Model for Alzheimer's Disease Studies. *Biomater.* **2013,** *34*, 2938-2946.
17. Frega, M.; Tedesco, M.; Massobrio, P.; Pesce, M.; Martinoia, S., Network Dynamics of 3D Engineered Neuronal Cultures: a New Experimental Model for In-Vitro Electrophysiology. *Sci. Rep.* **2014,** *4*, 5489.
18. Izsak, J.; Seth, H.; Andersson, M.; Vizlin-Hodzic, D.; Theiss, S.; Hanse, E.; Agren, H.; Funa, K.; Illes, S., Robust Generation of Person-Specific, Synchronously Active Neuronal Networks Using Purely Isogenic Human iPSC-3D Neural Aggregate Cultures. *Front. Neurosci.* **2019,** *13*, 351.
19. Wang, B.; Wang, L.; Tang, Y.; Shi, J.; Wei, J.; Tu, X.; Chen, Y., Fabrication of Spaced Monolayers of Electrospun Nanofibers for Three-Dimensional Cell Infiltration and Proliferation. *Microelectron. Eng.* **2018,** *198*, 73-77.
20. Woodruff, G.; Phillips, N.; Carromeu, C.; Guicherit, O.; White, A.; Johnson, M.; Zanella, F.; Anson, B.; Lovenberg, T.; Bonaventure, P.; Harrington, A. W., Screening for Modulators of Neural Network Activity in 3D Human iPSC-Derived Cortical Spheroids. *PLoS One* **2020,** *15*, e0240991.
21. Sundararaghavan, H. G.; Monteiro, G. A.; Firestein, B. L.; Shreiber, D. I., Neurite Growth in 3D Collagen Gels with Gradients of Mechanical Properties. *Biotechnol. Bioeng.* **2009,** *102*, 632-643.
22. Li, G. N.; Hoffman-Kim, D., Tissue-Engineered Platforms of Axon Guidance. *Tissue Eng. Part B Rev.* **2008,** *14*, 33-51.
23. Giandomenico, S. L.; Mierau, S. B.; Gibbons, G. M.; Wenger, L. M. D.; Masullo, L.; Sit, T.; Sutcliffe, M.; Boulanger, J.; Tripodi, M.; Derivery, E.; Paulsen, O.; Lakatos, A.; Lancaster, M. A., Cerebral Organoids at the Air-Liquid Interface Generate Diverse Nerve Tracts with Functional Output. *Nat. Neurosci.* **2019,** *22*, 669-679.

24. Rose, J. C.; Gehlen, D. B.; Omidinia-Anarkoli, A.; Folster, M.; Haraszti, T.; Jaekel, E. E.; De Laporte, L., How Much Physical Guidance is Needed to Orient Growing Axons in 3D Hydrogels? *Adv. Healthc. Mater.* **2020,** *9*, e2000886.
25. Qian, X.; Su, Y.; Adam, C. D.; Deutschmann, A. U.; Pather, S. R.; Goldberg, E. M.; Su, K.; Li, S.; Lu, L.; Jacob, F.; Nguyen, P. T. T.; Huh, S.; Hoke, A.; Swinford-Jackson, S. E.; Wen, Z.; Gu, X.; Pierce, R. C.; Wu, H.; Briand, L. A.; Chen, H. I.; Wolf, J. A.; Song, H.; Ming, G. L., Sliced Human Cortical Organoids for Modeling Distinct Cortical Layer Formation. *Cell Stem Cell* **2020,** *26*, 766-781.e9.
26. Trujillo, C. A.; Gao, R.; Negraes, P. D.; Gu, J.; Buchanan, J.; Preissl, S.; Wang, A.; Wu, W.; Haddad, G. G.; Chaim, I. A.; Domissy, A.; Vandenberghe, M.; Devor, A.; Yeo, G. W.; Voytek, B.; Muotri, A. R., Complex Oscillatory Waves Emerging from Cortical Organoids Model Early Human Brain Network Development. *Cell Stem Cell* **2019,** *25*, 558-569.e7.
27. Durens, M.; Nestor, J.; Williams, M.; Herold, K.; Niescier, R. F.; Lunden, J. W.; Phillips, A. W.; Lin, Y. C.; Dykxhoorn, D. M.; Nestor, M. W., High-Throughput Screening of Human Induced Pluripotent Stem Cell-Derived Brain Organoids. *J. Neurosci. Methods* **2020,** *335*, 108627.
28. Thomas, C. A., Jr.; Springer, P. A.; Loeb, G. E.; Berwald-Netter, Y.; Okun, L. M., A Miniature Microelectrode Array to Monitor the Bioelectric Activity of Cultured Cells. *Exp. Cell Res.* **1972,** *74*, 61-66.
29. Gross, G. W.; Williams, A. N.; Lucas, J. H., Recording of Spontaneous Activity with Photoetched Microelectrode Surfaces from Mouse Spinal Neurons in Culture. *J. Neurosci. Methods* **1982,** *5*, 13-22.
30. Connolly, P.; Clark, P.; Curtis, A. S.; Dow, J. A.; Wilkinson, C. D., An Extracellular Microelectrode Array for Monitoring Electrogenic Cells in Culture. *Biosens. Bioelectron.* **1990,** *5*, 223-234.
31. Heuschkel, M. O.; Fejtl, M.; Raggenbass, M.; Bertrand, D.; Renaud, P., A Three-Dimensional Multi-Electrode Array for Multi-Site Stimulation and Recording in Acute Brain Slices. *J. Neurosci. Methods* **2002,** *114*, 135-148.
32. Nam, Y.; Wheeler, B. C., In Vitro Microelectrode Array Technology and Neural Recordings. *Crit. Rev. Biomed. Eng.* **2011,** *39*, 45-61.
33. Bakkum, D. J.; Frey, U.; Radivojevic, M.; Russell, T. L.; Muller, J.; Fiscella, M.; Takahashi, H.; Hierlemann, A., Tracking Axonal Action Potential Propagation on a High-Density Microelectrode Array Across Hundreds of Sites. *Nat. Commun.* **2013,** *4*, 2181.
34. Hofmann, B.; Katelhon, E.; Schottdorf, M.; Offenhausser, A.; Wolfrum, B., Nanocavity Electrode Array for Recording from Electrogenic Cells. *Lab Chip* **2011,** *11*, 1054-1058.
35. Spira, M. E.; Hai, A., Multi-Electrode Array Technologies for Neuroscience and Cardiology. *Nat. Nanotechnol.* **2013,** *8*, 83-94.
36. Yakushenko, A.; Katelhon, E.; Wolfrum, B., Parallel On-Chip Analysis of Single Vesicle Neurotransmitter Release. *Anal. Chem.* **2013,** *85*, 5483-5490.
37. Wolfrum, B.; Katelhon, E.; Yakushenko, A.; Krause, K. J.; Adly, N.; Huske, M.; Rinklin, P., Nanoscale Electrochemical Sensor Arrays: Redox Cycling Amplification in Dual-Electrode Systems. *Acc. Chem. Res.* **2016,** *49*, 2031-2040.
38. Rastogi, S. K.; Bliley, J.; Shiwarski, D. J.; Raghavan, G.; Feinberg, A. W.; Cohen-Karni, T., Graphene Microelectrode Arrays for Electrical and Optical Measurements of Human Stem Cell-Derived Cardiomyocytes. *Cell Mol. Bioeng.* **2018,** *11*, 407-418.
39. Yeung, C. K.; Sommerhage, F.; Wrobel, G.; Offenhausser, A.; Chan, M.; Ingebrandt, S., Drug Profiling using Planar Microelectrode Arrays. *Anal. Bioanal. Chem.* **2007,** *387*, 2673-2680.

40. Johnstone, A. F.; Gross, G. W.; Weiss, D. G.; Schroeder, O. H.; Gramowski, A.; Shafer, T. J., Microelectrode Arrays: a Physiologically Based Neurotoxicity Testing Platform for the 21st Century. *Neurotoxicology* **2010,** *31*, 331-350.
41. Natarajan, A.; Stancescu, M.; Dhir, V.; Armstrong, C.; Sommerhage, F.; Hickman, J. J.; Molnar, P., Patterned Cardiomyocytes on Microelectrode Arrays as a Functional, High Information Content Drug Screening Platform. *Biomater.* **2011,** *32*, 4267-4274.
42. Czeschik, A.; Rinklin, P.; Derra, U.; Ullmann, S.; Holik, P.; Steltenkamp, S.; Offenhausser, A.; Wolfrum, B., Nanostructured Cavity Devices for Extracellular Stimulation of HL-1 Cells. *Nanoscale* **2015,** *7*, 9275-9281.
43. Latifi, S.; Tamayol, A.; Habibey, R.; Sabzevari, R.; Kahn, C.; Geny, D.; Eftekharpour, E.; Annabi, N.; Blau, A.; Linder, M.; Arab-Tehrany, E., Natural Lecithin Promotes Neural Network Complexity and Activity. *Sci. Rep.* **2016,** *6*, 25777.
44. Heer, F.; Franks, W.; Blau, A.; Taschini, S.; Ziegler, C.; Hierlemann, A.; Baltes, H., CMOS Microelectrode Array for the Monitoring of Electrogenic Cells. *Biosens. Bioelectron.* **2004,** *20*, 358-366.
45. Franke, F.; Jackel, D.; Dragas, J.; Muller, J.; Radivojevic, M.; Bakkum, D.; Hierlemann, A., High-Density Microelectrode Array Recordings and Real-Time Spike Sorting for Closed-Loop Experiments: an Emerging Technology to Study Neural Plasticity. *Front. Neural Circuits* **2012,** *6*, 105.
46. Muller, J.; Ballini, M.; Livi, P.; Chen, Y.; Radivojevic, M.; Shadmani, A.; Viswam, V.; Jones, I. L.; Fiscella, M.; Diggelmann, R.; Stettler, A.; Frey, U.; Bakkum, D. J.; Hierlemann, A., High-Resolution CMOS MEA Platform to Study Neurons at Subcellular, Cellular, and Network Levels. *Lab Chip* **2015,** *15*, 2767-2780.
47. Regehr, W. G.; Pine, J.; Cohan, C. S.; Mischke, M. D.; Tank, D. W., Sealing Cultured Invertebrate Neurons to Embedded Dish Electrodes Facilitates Long-Term Stimulation and Recording. *J. Neurosci. Methods* **1989,** *30*, 91-106.
48. Fair, S. R.; Julian, D.; Hartlaub, A. M.; Pusuluri, S. T.; Malik, G.; Summerfied, T. L.; Zhao, G.; Hester, A. B.; Ackerman, W. E. t.; Hollingsworth, E. W.; Ali, M.; McElroy, C. A.; Buhimschi, I. A.; Imitola, J.; Maitre, N. L.; Bedrosian, T. A.; Hester, M. E., Electrophysiological Maturation of Cerebral Organoids Correlates with Dynamic Morphological and Cellular Development. *Stem Cell Reports* **2020,** *15*, 855-868.
49. Santoro, F.; Dasgupta, S.; Schnitker, J.; Auth, T.; Neumann, E.; Panaitov, G.; Gompper, G.; Offenhausser, A., Interfacing Electrogenic Cells with 3D Nanoelectrodes: Position, Shape, and Size Matter. *ACS Nano* **2014,** *8*, 6713-6723.
50. Dipalo, M.; McGuire, A. F.; Lou, H. Y.; Caprettini, V.; Melle, G.; Bruno, G.; Lubrano, C.; Matino, L.; Li, X.; De Angelis, F.; Cui, B.; Santoro, F., Cells Adhering to 3D Vertical Nanostructures: Cell Membrane Reshaping without Stable Internalization. *Nano Lett.* **2018,** *18*, 6100-6105.
51. Santoro, F.; Schnitker, J.; Panaitov, G.; Offenhausser, A., On Chip Guidance and Recording of Cardiomyocytes with 3D Mushroom-Shaped Electrodes. *Nano Lett.* **2013,** *13*, 5379-5384.
52. Passaro, A. P.; Stice, S. L., Electrophysiological Analysis of Brain Organoids: Current Approaches and Advancements. *Front. Neurosci.* **2020,** *14*, 622137.
53. Shin, H.; Jeong, S.; Lee, J. H.; Sun, W.; Choi, N.; Cho, I. J., 3D High-Density Microelectrode Array with Optical Stimulation and Drug Delivery for Investigating Neural Circuit Dynamics. *Nat. Commun.* **2021,** *12*, 492.
54. Park, Y.; Franz, C. K.; Ryu, H.; Luan, H. W.; Cotton, K. Y.; Kim, J. U.; Chung, T. S.; Zhao, S. W.; Vazquez-Guardado, A.; Yang, D. S.; Li, K.; Avila, R.; Phillips, J. K.; Quezada, M. J.; Jang, H.; Kwak, S. S.; Won, S. M.; Kwon, K.; Jeong, H.; Bandodkar, A. J.; Han, M. D.; Zhao, H. B.; Osher, G. R.; Wang, H. L.; Lee, K.; Zhang, Y. H.; Huang, Y.

G.; Finan, J. D.; Rogers, J. A., Three-Dimensional, Multifunctional Neural Interfaces for Cortical Spheroids and Engineered Assembloids. *Sci. Adv.* **2021,** *7*, eabf9153.
55. Soscia, D. A.; Lam, D.; Tooker, A. C.; Enright, H. A.; Triplett, M.; Karande, P.; Peters, S. K. G.; Sales, A. P.; Wheeler, E. K.; Fischer, N. O., A Flexible 3-Dimensional Microelectrode Array for In Vitro Brain Models. *Lab Chip* **2020,** *20*, 901-911.
56. Campbell, P. K.; Jones, K. E.; Huber, R. J.; Horch, K. W.; Normann, R. A., A Silicon-Based, Three-Dimensional Neural Interface: Manufacturing Processes for an Intracortical Electrode Array. *IEEE Trans. Biomed. Eng.* **1991,** *38*, 758-768.
57. Chu, H. Y.; Kuo, T. Y.; Chang, B. W.; Lu, S. W.; Chiao, C. C.; Fang, W. L., Design and Fabrication of Novel Three-Dimensional Multi-Electrode Array Using SOI Wafer. *Sens. Actuator A Phys.* **2006,** *130*, 254-261.
58. Charvet, G.; Rousseau, L.; Billoint, O.; Gharbi, S.; Rostaing, J. P.; Joucla, S.; Trevisiol, M.; Bourgerette, A.; Chauvet, P.; Moulin, C.; Goy, F.; Mercier, B.; Colin, M.; Spirkovitch, S.; Fanet, H.; Meyrand, P.; Guillemaud, R.; Yvert, B., BioMEA: a Versatile High-Density 3D Microelectrode Array System using Integrated Electronics. *Biosens. Bioelectron.* **2010,** *25*, 1889-1896.
59. Saleh, M. S.; Hu, C. S.; Panat, R., Three-Dimensional Microarchitected Materials and Devices using Nanoparticle Assembly by Pointwise Spatial Printing. *Sci. Adv.* **2017,** *3* e1601986.
60. Grob, L.; Yamamoto, H.; Zips, S.; Rinklin, P.; Hirano-Iwata, A.; Wolfrum, B., Printed 3D Electrode Arrays with Micrometer-Scale Lateral Resolution for Extracellular Recording of Action Potentials. *Adv. Mater. Technol.* **2020,** *5*, 1900517.
61. Zips, S.; Grob, L.; Rinklin, P.; Terkan, K.; Adly, N. Y.; Weiss, L. J. K.; Mayer, D.; Wolfrum, B., Fully Printed µ-Needle Electrode Array from Conductive Polymer Ink for Bioelectronic Applications. *ACS Appl. Mater. Interfaces* **2019,** *11*, 32778-32786.
62. Huang, B.; Peng, J.; Huang, X.; Liang, F.; Wang, L.; Shi, J.; Yamada, A.; Chen, Y., Generation of Interconnected Neural Clusters in Multiscale Scaffolds from Human-Induced Pluripotent Stem Cells. *ACS Appl. Mater. Interfaces* **2021,** *13*, 55939-55952.
63. Tang, Y.; Liu, L.; Li, J.; Yu, L.; Severino, F. P. U.; Wang, L.; Shi, J.; Tu, X.; Torre, V.; Chen, Y., Effective Motor Neuron Differentiation of hiPSCs on a Patch Made of Crosslinked Monolayer Gelatin Nanofibers. *J. Mater. Chem. B* **2016,** *4*, 3305-3312.
64. Huang, B.; He, Y.; Rofaani, E.; Liang, F.; Huang, X.; Shi, J.; Wang, L.; Yamada, A.; Peng, J.; Chen, Y., Automatic Differentiation of Human Induced Pluripotent Stem Cells toward Synchronous Neural Networks on an Arrayed Monolayer of Nanofiber Membrane. *Acta Biomater.* **2022,** *150*, 168-180.
65. Gunhanlar, N.; Shpak, G.; van der Kroeg, M.; Gouty-Colomer, L. A.; Munshi, S. T.; Lendemeijer, B.; Ghazvini, M.; Dupont, C.; Hoogendijk, W. J. G.; Gribnau, J.; de Vrij, F. M. S.; Kushner, S. A., A Simplified Protocol for Differentiation of Electrophysiologically Mature Neuronal Networks from Human Induced Pluripotent Stem Cells. *Mol. Psychiatry* **2018,** *23*, 1336-1344.
66. Giandomenico, S. L.; Sutcliffe, M.; Lancaster, M. A., Generation and Long-Term Culture of Advanced Cerebral Organoids for Studying Later Stages of Neural Development. *Nat. protoc.* **2021,** *16*, 579-602.
67. Donoho, D. L.; Johnstone, I. M., Ideal Spatial Adaptation by Wavelet Shrinkage. *Biometrika* **1994,** *81*, 425-455.
68. Quiroga, R. Q.; Nadasdy, Z.; Ben-Shaul, Y., Unsupervised Spike Detection and Sorting with Wavelets and Superparamagnetic Clustering. *Neural Comput.* **2004,** *16*, 1661-1687.

69. Sloan, S. A.; Andersen, J.; Pasca, A. M.; Birey, F.; Pasca, S. P., Generation and Assembly of Human Brain Region-Specific Three-Dimensional Cultures. *Nat. protoc.* **2018,** *13*, 2062-2085.
70. Anastasaki, C.; Wilson, A. F.; Chen, A. S.; Wegscheid, M. L.; Gutmann, D. H., Generation of Human Induced Pluripotent Stem Cell-Derived Cerebral Organoids for Cellular and Molecular Characterization. *STAR Protoc.* **2022,** *3*, 101173.
71. Bianchi, M.; Carli, S.; Lauro, M. D.; Prato, M.; Murgia, M.; Fadigaad, L.; Biscariniae, F., Scaling of Capacitance of PEDOT:PSS: Volume vs. Area. *J. Mater. Chem. C* **2020,** *8*, 11252-11262.
72. Obien, M. E.; Deligkaris, K.; Bullmann, T.; Bakkum, D. J.; Frey, U., Revealing Neuronal Function through Microelectrode Array Recordings. *Front. Neurosci.* **2014,** *8*, 423.
73. Saleh, M. S.; Ritchie, S. M.; Nicholas, M. A.; Gordon, H. L.; Hu, C.; Jahan, S.; Yuan, B.; Bezbaruah, R.; Reddy, J. W.; Ahmed, Z.; Chamanzar, M.; Yttri, E. A.; Panat, R. P., CMU Array: A 3D Nanoprinted, Fully Customizable High-Density Microelectrode Array Platform. *Sci. Adv.* **2022,** *8*, eabj4853.
74. Peng, H.; Grob, L.; Weiss, L. J. K.; Hiendlmeier, L.; Music, E.; Kopic, I.; T, F. T.; Rinklin, P.; Wolfrum, B., Inkjet-Printed 3D Micro-Ring-Electrode Arrays for Amperometric Nanoparticle Detection. *Nanoscale* **2023,** *15*, 4006-4013.

TOC graphic

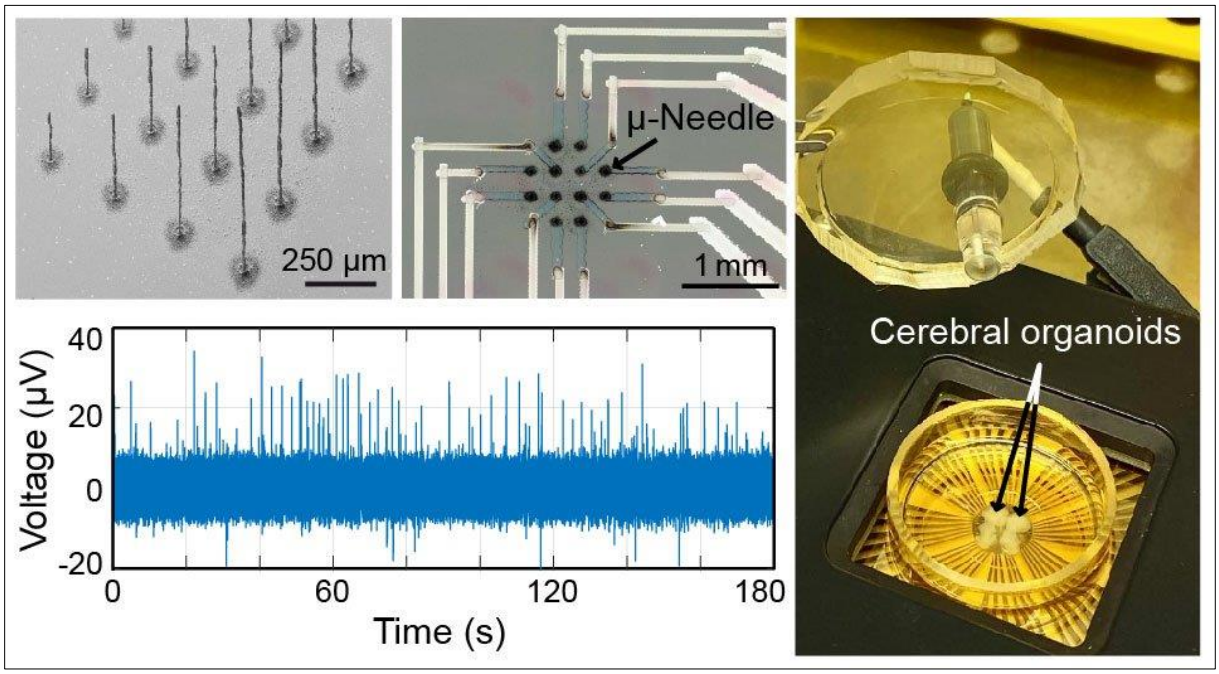

Supporting Information

Figures S1-S4

Aerosol jet-Printed High-Aspect Ratio Micro-Needle Electrode Arrays Applied for Human Cerebral Organoids and 3D Neurospheroid Networks

Sabine Zips[1]‡, Boxin Huang[2†]‡, Salammbô Hotte[2†]‡, Lukas Hiendlmeier[1], Chen Wang[1], Karthyayani Rajamani[2], Olivier Buriez[2], George Al Boustani,[1] Yong Chen[2], Bernhard Wolfrum[1]*, Ayako Yamada[2]**

[1] Neuroelectronics - Munich Institute of Biomedical Engineering, Department of Electrical Engineering, TUM School of Computation, Information and Technology, Technical University of Munich, Boltzmannstr. 11, 85748 Garching, Germany

[2] PASTEUR, Department of Chemistry, École Normale Supérieure, PSL University, Sorbonne Université, CNRS, 75005 Paris, France

Corresponding authors

*Yong Chen, email: yong.chen@ens.psl.eu

*Bernhard Wolfrum, email: bernhard.wolfrum@tum.de

*Ayako Yamada, email: ayako.yamada@ens.psl.eu

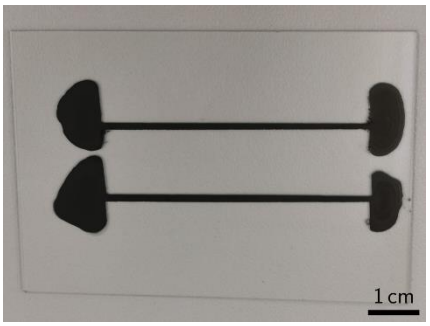

Figure S1. Example electrodes used to measure the conductivity of the improved PEDOT:PSS-MWCNT ink.

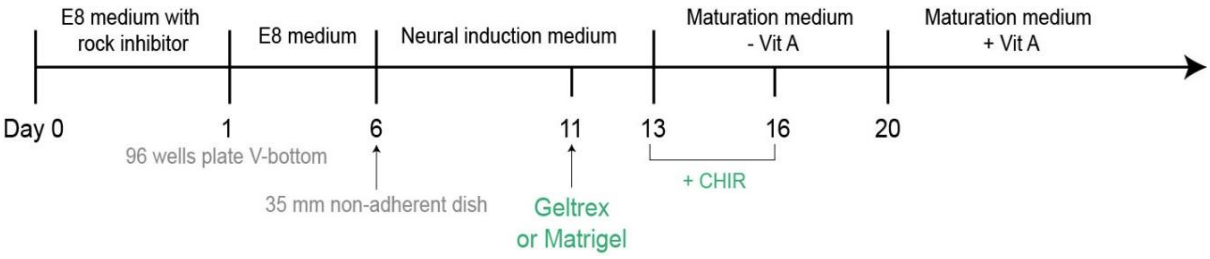

Figure S2. Timeline of the hiPSC differentiation into cerebral organoids.

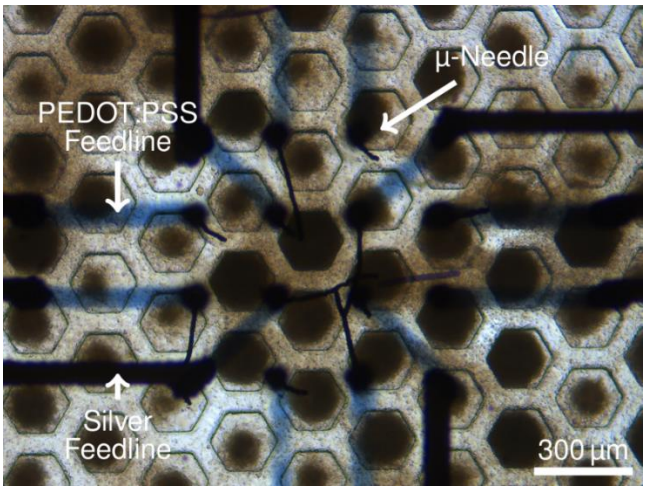

Figure S3. Bright field microscopy image of one of the central electrode areas on an MnEA with an integrated micro-honeycomb substrate with neurospheroids.

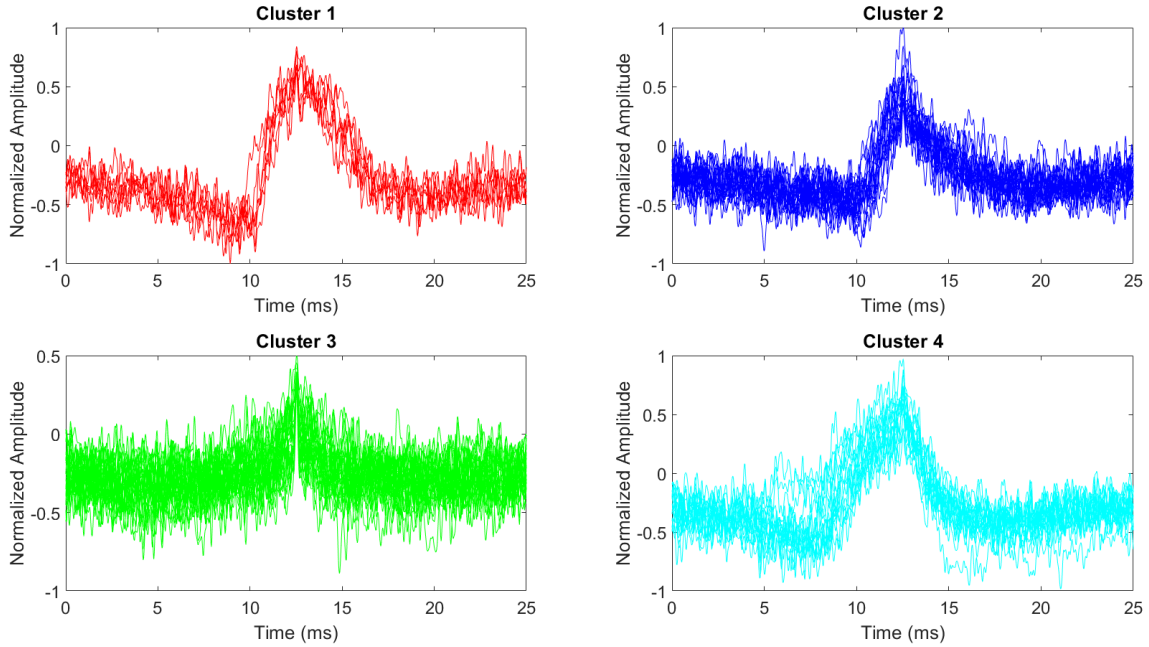

Figure S4. Clusters of individual peak shapes recorded in the measurements on cerebral organoids. The graphs were obtained after applying a bandpass filter between 50 Hz and 4 kHz. Subsequent to spike detection, features were extracted using principal component analysis. The feature vectors were clustered in four groups representing similar features. The analysis was conducted using Matlab.